Robust organelle size control via bursty growth

Kiandokht Panjtan Amiri[1,*], Asa Kalish[1,*], & Shankar Mukherji[1,2,3]

[1]Department of Physics, Washington University in St. Louis, St. Louis, MO

[2]Department of Cell Biology Physiology, Washington University School of Medicine, St. Louis, MO

[3]Center for the Science and Engineering of Living Systems, McKelvey School of Engineering, Washington University in St. Louis, St. Louis, MO

Correspondence to: smukherji@wustl.edu

[*]These authors contributed equally

Abstract

Among the most important processes in the self-assembly of the eukaryotic cell is the synthesis of its organelles, specialized biochemical compartments that house processes crucial to cellular physiology. A critical property that governs organelle function is its size. Numerous molecular factors that regulate the sizes of a diverse array of organelles, including the Golgi, mitochondria, peroxisomes and lipid droplets among others, have been identified. However, our understanding of the quantitative principles governing organelle size control remains incomplete. Here, we combine organelle size data from the single-celled eukaryote *Saccharomyces cerevisiae* and mathematical theory to show that cells can robustly control organelle size fluctuations across a range of organelle sizes. In particular, our framework suggests that organelle size increases in random bursts from a limited pool of building blocks. Bursty organelle growth allows the cell to decouple the average magnitude of organelle size fluctuations from mean organelle size, provided the bursts do not deplete the pool of building blocks from which organelles grow. Bursty growth thus provides a potentially general mechanism by which cells can regulate the noise of the sizes of its subcellular structures.

Organelle size is affected by both size-specific processes, such as growth and disassembly, as well as number changing processes such as fission and fusion[1,2]. To analyze how these processes govern organelle size, we developed a stochastic model of organelle growth to compute the joint probability distribution of organelle numbers and sizes in single cells. In this model we assume that organelles are created de novo, decay, undergo fission and fusion, grow in size, and shrink (**Fig.1a**). Using the Gillespie algorithm[3] we solve our model for the three general limits that organelle growth can take. In the first limit, which we term constant growth, we assume that the pool of building blocks is unlimited, and that growth occurs at a constant rate. In the second limit, which we term negative feedback control, we assume that the pool of building blocks is unlimited, however the cell imposes a constraint on organelles that drives them towards a target size. In the third limit, which we term the limiting pool, we assume that organelle sizes are constrained by a limited pool of building blocks from which they are assembled. The simulation is performed by tracking the abundance (**N**) and sizes (**s**) of organelles in a single cell, from t = 0 until **N** and the mean organelle size **<s>** reach steady state; example trajectories of each of the three organelle growth limits are shown (**Fig. 1b-1d, Supplementary Figure. 2a-2f**). We repeat these simulations for 1000 cells and extract **N** and **<s>** from each simulated cell. Inspired by physiologically-relevant cases, we focused the simulations on three different regimes of number changing dynamics: in the late Golgi[4,5] and lipid droplet[6-8] relevant case in which number dynamics are governed by de novo synthesis and first order decay (**Fig. 1e**), in the peroxisome relevant limit of when organelle numbers change through de novo synthesis, first order decay, and fission[9-11] (**Fig. 1f**), and lastly in the mitochondria relevant limit of when the abundance of organelles changes solely through fission and fusion[12] (**Fig. 1g**). In each regime we focus on the correlation between organelle abundance and average organelle size from cells with **N** organelles, $\langle s \rangle_N$. Most importantly, we note that in the limiting pool limit we expect a negative correlation between **N** and $\langle s \rangle_N$ in both de novo synthesis and fission dominated organelle number controlling regimes, while in the constant growth regime the negative correlation between **N** and $\langle s \rangle_N$ exists only when organelle numbers can increase by fission and should flatten upon reduction in fission (**Supplementary Figure. 2g-2i**). Furthermore, we note that in the case of fission and fusion dominated copy numbers, the constant growth and limited pool limits both reduce to the same picture as the fission and fusion processes conserve biomass that thus limits the size of organelles upon an increase in copy number.

We next use our model in conjunction with endogenous stochastic fluctuations in organelle numbers and sizes to infer organelle growth rules in the budding yeast *Saccharomyces cerevisiae*. To visualize the various organelles we examine, we fuse the fluorescent protein monomeric Kusibara Orange2 (mKO2) to organelle membrane resident proteins. We obtain **<s>** vs. **N** distributions of fluorescently labelled late Golgi (labelled with Sec7-mKO2), lipid droplets (Erg6-mKO2), peroxisomes (Pex3-mKO2), and mitochondria (Tom70-mKO2) and from these joint distributions plot $\langle s \rangle_N$ as a function of **N**. For each of the organelles we examine, we observe a significant negative correlation between **N** and $\langle s \rangle_N$ (**Fig. 1h-1k**). In the case of late Golgi and lipid droplets, which we expect are dominated by de novo synthesis, the negative correlation is inconsistent with the constant growth and negative feedback limits of the general stochastic growth model. In the case of the mitochondria, whose copy numbers are a result of fission and fusion, the observed negative correlation is inconsistent with negative feedback. In the case of the peroxisome, the negative correlation is consistent with both constant growth with fission and the limiting pool limits. In order to distinguish between these pictures, we note that reducing peroxisome fission should flatten the $\langle s \rangle_N$ vs. **N** curve if peroxisome growth occurs in the constant growth limit while it should remain negatively correlated in the limiting pool limit. We genetically deleted the peroxisome fission factors *DNM1, FIS1,* and *VPS1*[13,14] (**Supplementary Figure. 2j-2l**) and observe a negative correlation between $\langle s \rangle_N$ and **N**, inconsistent with constant growth and negative feedback as the underlying mechanisms of size control. Our measurements suggest that the size of these organelles is constrained by a limited pool of building blocks.

Among the most attractive hypotheses arguing for the utility of the limiting pool model of organelle growth is that it achieves a stable organelle size in the absence of feedback. However, it has been shown theoretically that growing multiple organelles from a limited pool of building blocks can lead to severe size fluctuations between organelles within the same cell[15], potentially impairing cellular-scale physiological function. To quantify how growth from a limited pool affects intracellular fluctuations in organelle size in our model, we plot the average coefficient of variation (CV) in organelle size as a function of $\langle s \rangle_N$ from the cells simulated in the limiting pool limit of the model (**Fig. 1l-o**, blue dots). Similar to previous work, we observe that for decreasing $\langle s \rangle_N$ (or increasing **N**) the intracellular organelle size CV increases. We then use our experimental joint distributions of organelle number and size for the late Golgi, lipid droplets, mitochondria and peroxisomes to directly measure the CV of organelle sizes within single cells, (**Fig. 1l-o**). Contrary to our theoretical expectation (**Fig. 1l-o**, insets), we see that the average intracellular CV of the late Golgi, lipid droplets and peroxisomes remain constant with varying average organelle size. Only the average intracellular CV of mitochondria appears to increase when the cell creates more, smaller copies of this organelle.

To address the discrepancy between the noise profile resulting from our model versus the noise profile of organelles observed experimentally, we consider a fundamental revision to how organelle growth proceeds in our mathematical framework. Building on previous observations that subcellular structures can grow from bursts of random sizes of building blocks[16] we constructed a model in which organelles grow from a limited pool of building blocks in exponentially distributed bursts of random size β that occur at random times characterized by a burst frequency α (**Fig. 2a**). In this model, if the limited pool of building blocks is not exhausted, thus allowing the different organelles within a cell to fluctuate in size statistically independently of one another, and if copy number changes are slow compared to size changes, then the resulting organelle sizes from cells that contain a defined number of organelles **N** follow a gamma distribution with mean size $\alpha\beta$. Crucially, the average intracellular CV of gamma distributed organelle sizes would depend only on the burst frequency α but be independent of the burst size β [17], thus allowing the cell to decouple the average intracellular organelle size CV from the mean organelle size by appropriately changing α and β. Unlike when organelles grow through deterministically sized

steps, if organelle growth from the limited pool only reduces β to decrease average organelle size, but leaves α unchanged, then bursty organelle growth from an undepleted pool results in gamma distributed organelle sizes (**Fig. 2b**), and the average intracellular organelle size CV becoming independent of the average organelle size (**Fig. 2c**). However, if the limited pool does deplete, then organelles compete for the building blocks, leading to anti-correlated fluctuations in organelle size and increases in the average intracellular CV (**Fig. 2d**). This model thus makes two predictions we can experimentally test: if the pool of building blocks is not depleted, the organelle size distributions should be gamma distributed with only β changing and α remaining constant between subpopulations of cells with different N, and if the pool depletes we should observe a rise in the average intracellular CV.

To test our hypothesis of bursty organelle growth for our organelle size data we first construct a measure of pool depletion. To measure pool depletion, we measure $\mathbf{V} = \langle \mathbf{s} \rangle_{\mathbf{N}} * \mathbf{N}$, the total organelle biomass, and assume all cells have roughly equal amounts of the limiting pool. Plotting **V** as a function of **N**, if **V** increases with the number of organelles, we conclude that the pool has not depleted. However, if at higher organelle numbers **V** plateaus then we conclude that the limited pool has depleted. Next, we fit the single organelle size distributions from cells with a given N to gamma distributions and extract the burst frequency α and burst size β. We plot the **V** versus **N** and α versus β for the late Golgi body, lipid droplets and peroxisomes.

We observe that while the late Golgi, lipid droplet, and peroxisomes each grow from a limited pool, the pool does not appear to deplete (**Fig. 3a,d,g**). Fitting gamma distributions to late Golgi, lipid droplet, and peroxisome size histograms for cells with different number of these organelles (**Fig. 3b,e,h, Supplementary Figure. 4**), we see that the α remains constant while β decreases as organelle number increases (**Fig. 3c,f,i**). As the CV of our gamma distribution is $1/\sqrt{\alpha}$, our model and the relatively constant average intracellular CV suggest that the Golgi apparatus, lipid droplet, and peroxisomes grow in exponentially distributed bursts from a limited pool of building blocks.

To test our prediction that organelle growth from a limited pool with no spare capacity leads to an elevated intracellular CV, we examine the case of mitochondria, whose sizes are a balance between biomass conserving fission and fusion. We plot **V** vs. **N** for mitochondria and observe a flat line (**Supplementary Fig.5a**), consistent with the idea that cells largely rearrange existing a fixed pool of mitochondrial biomass when changing mitochondrial **N** through fission and fusion. The resulting organelle size distributions are consistent with our model (**Supplementary Fig. 5c-i**) and with our observation that an increasing intracellular CV with decreasing mitochondria size (**Fig. 1o**).

To test our prediction that lowering the burst frequency will increase average intracellular size fluctuations, we reason that inhibiting large bursts of size changes in the Golgi from vesicular traffic would lead to a narrower distribution of burst sizes that would mimic deterministic growth steps and lead to an increased average intracellular Golgi CV similar to the prediction of our original model. To test this idea, we analyze the late Golgi in cells lacking the vesicular traffic regulator *ARF1*[18]. We observe, in agreement with our hypothesis, that upon deletion of *ARF1* the average intracellular Golgi size CV increases as the average Golgi size decreases (**Fig. 4a-4b**).

Finally, to test our prediction that pool depletion leads to an elevated intracellular organelle size CV, we turn to lipid droplets and peroxisomes. Lipid droplets and peroxisomes are dynamic organelles whose sizes and copy numbers increase upon cellular exposure to long chain fatty acid-rich environments[7,8,19]. We hypothesized that culturing cells in an oleic acid rich environment

could expose capacity constraints in lipid droplet and peroxisome biogenesis given our previous observation that these organelles appear to grow from a limited pool of building blocks. We observe that when grown in glucose, neither lipid droplets nor peroxisomes deplete the limited pool of building blocks, however, when grown in medium rich in oleic acid, V plateaus (**Fig. 4c,e**), suggesting that the pool has depleted. Concomitantly, we observe that the lipid droplet and peroxisome average intracellular organelle size CV increases with decreasing $\langle s \rangle_N$ (**Fig. 4d,f**). Importantly, we observe the elevation of the average intracellular peroxisome size CV in oleic acid even upon deletion of the primary peroxisome fission factor *VPS1*, (**Fig. 4f**) suggesting that capacity constraints from the limited pool of building blocks, and not elevated fission, are responsible for the increased noise in peroxisome sizes.

Through the disagreement of our measurement of average intracellular organelle size fluctuations and a simple model of organelle size control based on deterministic growth step sizes, we propose a model in which organelle growth proceeds in a burst-like fashion. The underlying molecular mechanisms producing these bursts are yet to be revealed and are likely to be organelle-specific: Golgi size, for example, will be influenced by both small increases in size from non-vesicular traffic as well as sudden, large increases in size from vesicle fusion while lipid droplet size bursts may result from bursty expression of genes such as those encoding neutral lipid synthesis enzymes. However, the size statistics of a diverse array of organelles appear to be well described by a single unifying model that can be used to interpret future studies on the mechanistic underpinnings of organelle size control and a basis for more sophisticated modeling efforts to more accurately capture details suppressed here[20,21]. Our results point to the potentially general principle that that robust size control can, remarkably, be the result of random burst-like assembly of subcellular structures.

References

1. Rafelski, S. M. & Marshall, W. F. Building the cell: design principles of cellular architecture. *Nature Reviews Molecular Cell Biology* 9, 593 (2008).
2. Lowe, M. & Barr, F. A. Inheritance and biogenesis of organelles in the secretory pathway. *Nature Reviews Molecular Cell Biology* 8, 429 (2007).
3. Gillespie, D. T. Exact stochastic simulation of coupled chemical reactions. *The journal of physical chemistry* 81, 2340–2361 (1977).
4. Bevis, B. J., Hammond, A. T., Reinke, C. A. & Glick, B. S. De novo formation of transitional ER sites and Golgi structures in *Pichia pastoris*. *Nature cell biology* 4, 750 (2002).
5. Rossanese, O. W. *et al.* Golgi structure correlates with transitional endoplasmic reticulum organization in pichia pastoris and saccharomyces cerevisiae. *The Journal of cell biology* 145, 69–81 (1999).
6. Pol, A., Gross, S. P. & Parton, R. G. Biogenesis of the multifunctional lipid droplet: lipids, proteins, and sites. *J Cell Biol* 204, 635–646 (2014).
7. Wilfling, F., Haas, J. T., Walther, T. C. & Farese Jr, R. V. Lipid droplet biogenesis. *Current opinion in cell biology* 29, 39–45 (2014).
8. Walther, T. C., Chung, J. & Farese Jr, R. V. Lipid droplet biogenesis. *Annual review of cell and developmental biology* 33, 491–510 (2017).
9. Hoepfner, D., Schildknegt, D., Braakman, I., Philippsen, P. & Tabak, H. F. Contribution of the endoplasmic reticulum to peroxisome formation. *Cell* 122, 85–95 (2005).
10. Van Der Zand, A., Gent, J., Braakman, I. & Tabak, H. F. Biochemically distinct vesicles from the endoplasmic reticulum fuse to form peroxisomes. *Cell* 149, 397–409 (2012).
11. Motley, A. M. & Hettema, E. H. Yeast peroxisomes multiply by growth and division. *The Journal of cell biology* 178, 399–410 (2007).
12. Diaz, F. & Moraes, C. T. Mitochondrial biogenesis and turnover. *Cell calcium* 44, 24–35 (2008).
13. Kuravi, K. *et al.* Dynamin-related proteins Vps1p and Dnm1p control peroxisome abundance in saccharomyces cerevisiae. *Journal of cell science* 119, 3994–4001 (2006).
14. Mukherji, S. & O'Shea, E. K. Mechanisms of organelle biogenesis govern stochastic fluctuations in organelle abundance. *Elife* 3, e02678 (2014).
15. Mohapatra, L., Lagny, T. J., Harbage, D., Jelenkovic, P. R. & Kondev, J. The limiting-pool mechanism fails to control the size of multiple organelles. *Cell systems* 4, 559–567 (2017).
16. Ludington, W. B., Wemmer, K. A., Lechtreck, K. F., Witman, G. B. & Marshall, W. F. Avalanche-like behavior in ciliary import. *Proceedings of the National Academy of Sciences* 110, 3925–3930 (2013).
17. Friedman, N., Cai, L. & Xie, X. S. Linking stochastic dynamics to population distribution: an analytical framework of gene expression. *Physical review letters* 97, 168302 (2006).
18. Bhave, M. *et al.* Golgi enlargement in arf-depleted yeast cells is due to altered dynamics of cisternal maturation. *J Cell Sci* 127, 250–257 (2014).
19. Mast, F. D., Fagarasanu, A., Knoblach, B. & Rachubinski, R. A. Peroxisome biogenesis: something old, something new, something borrowed. *Physiology* 25, 347–356 (2010).
20. Craven, C. J. Evaluation of predictions of the stochastic model of organelle production based on exact distributions. *Elife* 5, e10167 (2016).
21. Choubey, S., Das, D. & Majumdar, S. Cell-to-cell variability in organelle abundance reveals mechanisms of organelle biogenesis. *Physical Review E* 100, 022405 (2019).

Figure Captions

Fig 1. a) Schematic of mathematical framework. De novo synthesis of organelles, fission, fusion, organelle growth, shrink, and organelle decay occur at rate constants k_{denovo}, $k_{fission}$, k_{fusion}, k_{grow}, k_{shrink}, and γ respectively. In the regime where organelle abundances change through de novo synthesis and first order decay **b**) trace of a simulated single cell in the regime of constant growth **c**) negative feedback control, and **d**) limiting pool, from t = 0 (circle) to steady-state (square). Average of mean organelle sizes $\langle s \rangle_N$ vs. number of organelles **N** from 1000 simulated cells at steady state in a regime where organelle abundances change through **e**) de novo synthesis and first order decay, **f**) de novo synthesis, fission, and first order decay, and **g**) fission and fusion. The red, green, and blue dots correspond to the constant growth, negative feedback, and limiting pool regime of our model. Experimental measurements of $\langle s \rangle_N$ vs. **N** for fluorescently labelled **h**) Golgi body, **i**) lipid droplets, **j**) peroxisomes, and **k**) mitochondria. Average coefficient of variation (CV) of intracellular organelle sizes $\langle s \rangle_N$ for **l**) late Golgi, **m**) lipid droplets, **n**) peroxisomes, and **o**) mitochondria; insets represent the predicted CV from our limiting pool model, and the red dots correspond to CVs of fluorescently labelled

Fig 2. a) Schematic of the deterministic versus bursty model of organelle size control. **b**) Histogram of organelle sizes resulting from bursty model simulation. Black line represents the best fit of a gamma distribution to organelle size distributions. **c**) Average CV of organelle sizes in 1000 simulated cells from bursty model, when pool is not depleted. **d**) Average CV of organelle sizes in 1000 simulated cells from bursty model, when pool is depleted.

Fig 3. Biomass (**V**) as a function of number of organelles **N**, histograms of absolute organelle sizes in a sample subpopulation with fixed **N**, and inferred burst size and frequency parameters for **a-c**) late Golgi, **d-f**) lipid droplets, and **g-i**) peroxisomes in wildtype yeast cells. The black lines in **b**, **e**, and **h** represent the best fit gamma distribution to the experimentally measured organelle size histograms.

Fig 4. a) Biomass **V** and **b**) average intracellular size CV of late Golgi from populations of wildtype (magenta) and *ΔARF1* (purple) cells. **c**) Biomass **V** and **d**) average intracellular size CV of lipid droplets from populations of wildtype cells grown in glucose (magenta) and in medium rich in oleic acid (pink). **e**) Biomass **V** and **f**) average intracellular size CV of peroxisomes from populations of wildtype cells grown in glucose (magenta) and of wildtype (pink) and *ΔVPS1* (purple) cells grown in medium rich in oleic acid.

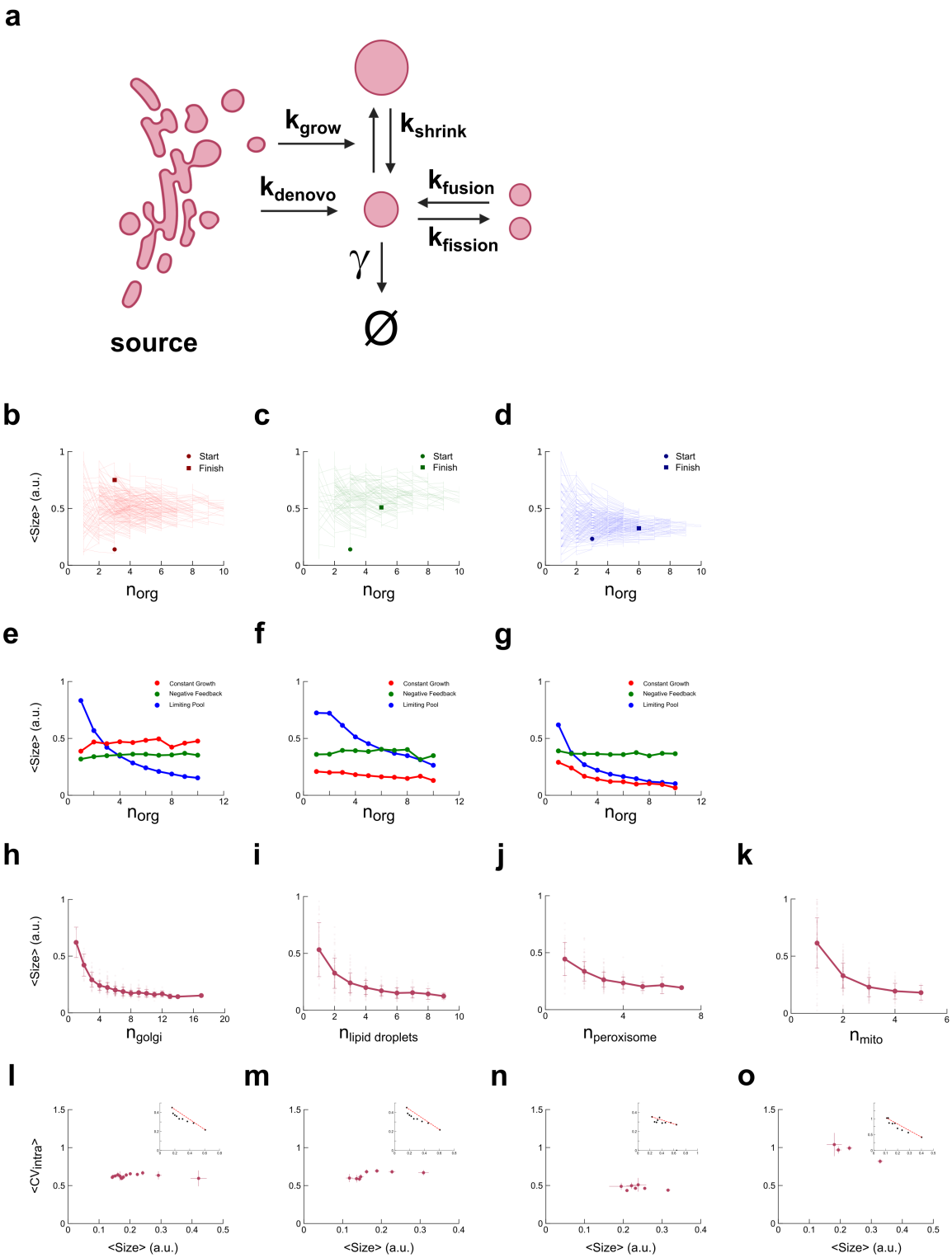

Panjtan Amiri, Kalish, and Mukherji – Figure 1

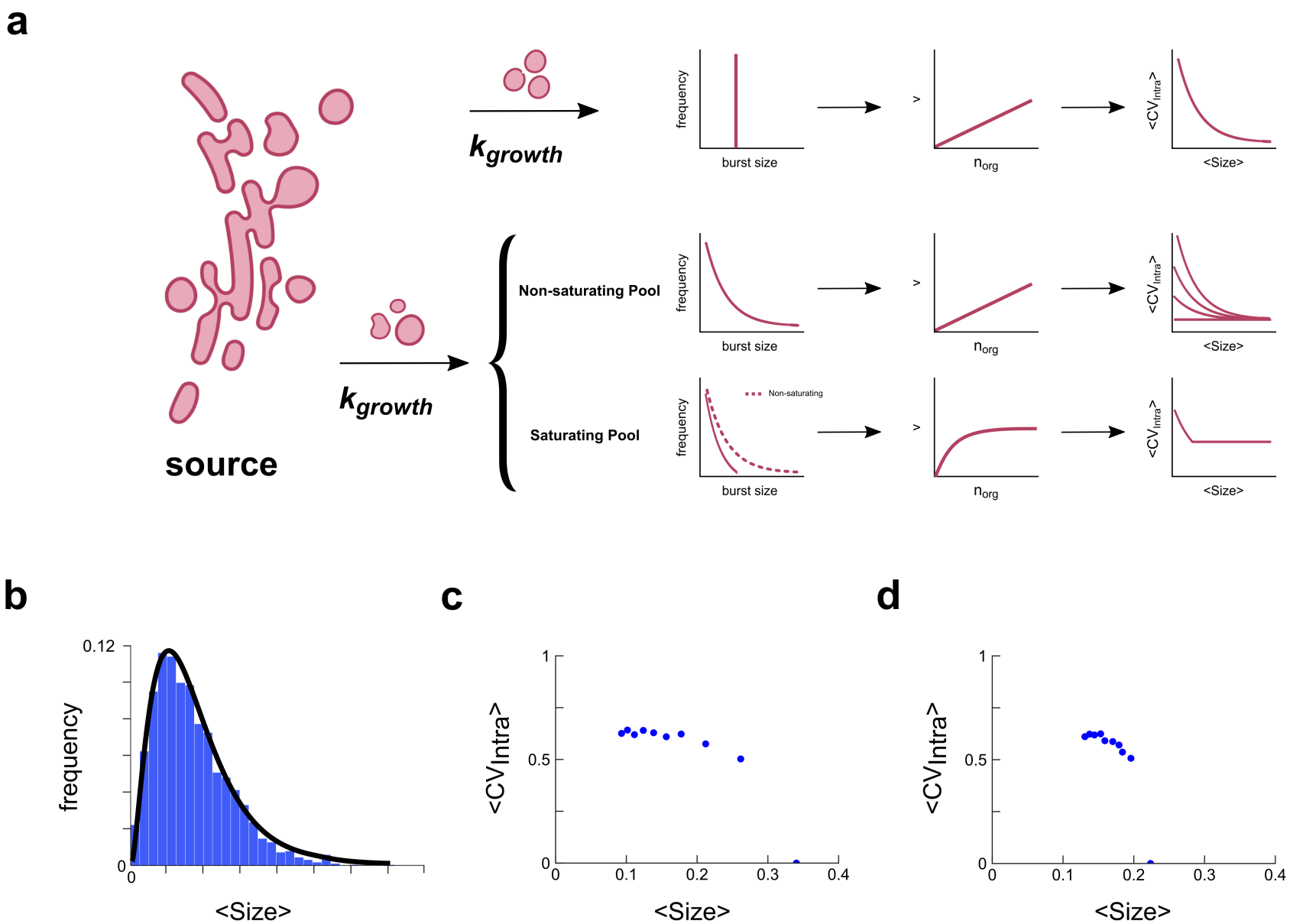

Panjtan Amiri, Kalish, and Mukherji – Figure 2

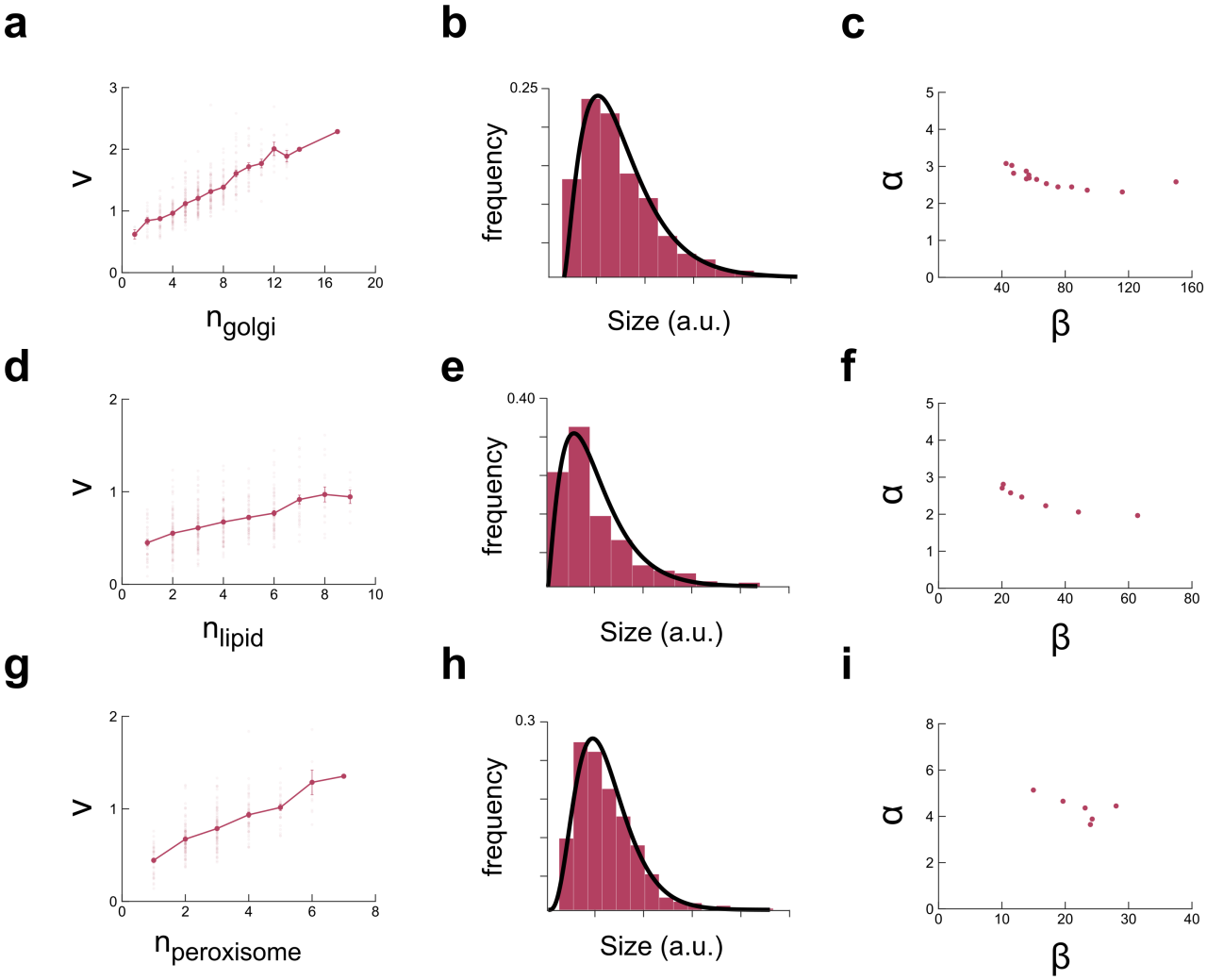

Panjtan Amiri, Kalish, and Mukherji – Figure 3

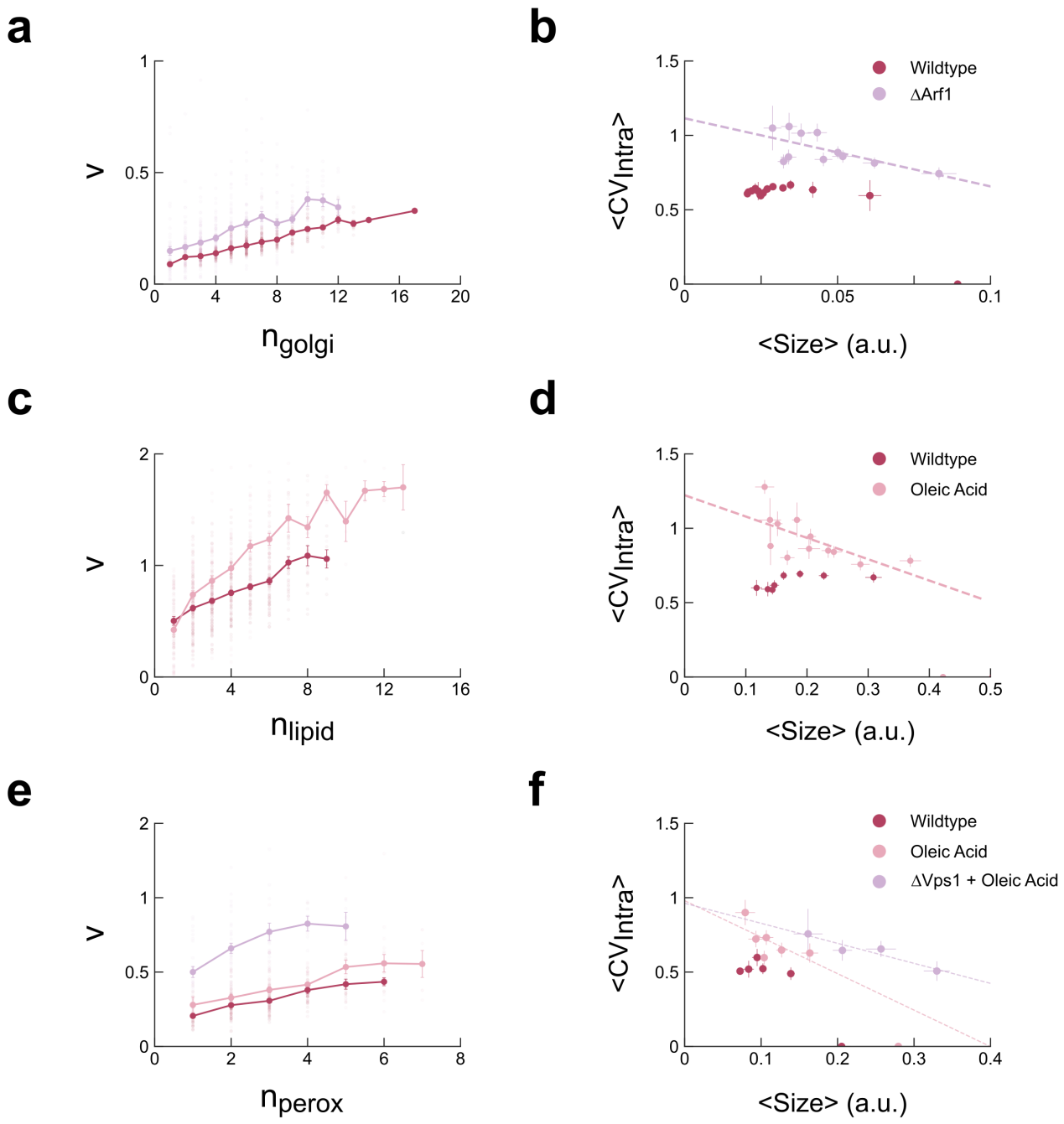

Panjtan Amiri, Kalish, and Mukherji – Figure 4

Supplementary Material

Materials and Methods Strains

Saccharomyces cerevisiae strain BY4742 was obtained as a kind gift from H. Zaher. Cells were transformed by standard lithium acetate methods to fluorescently labelled indicated organelles with monomeric Kusibara Orange 2 (mKO2) obtained from Addgene (Cambridge, MA). Peroxisomes in strains engineered with deletions of *DNM1, FIS1,* and *VPS1* were visualized as in Ref. 1.

Culture conditions

For glucose medium, strains were grown to mid-log phase at 30˚C in standard synthetic medium containing 2% glucose and subsequently imaged. For oleic acid medium, strains were grown to mid-log phase at 30˚C in standard synthetic medium containing 2% glucose, washed twice, and resuspended in medium containing 0.3% yeast extract, 0.6% peptone, 0.1% glucose, 0.1% Tween40, and 0.2% oleic acid, cultured for 20 hours in the oleic acid rich medium, and subsequently imaged.

Imaging Conditions

Wildtype strains were imaged with a Nikon Ti2 microscope using a Hamamatsu Orca Flash v3 scientific CMOS camera with standard TRITC emission and excitation filter cubes. The exposure time for the samples ranged from 50 - 250ms. Strains engineered with deletions of *DNM1, FIS1,* and *VPS1* were imaged as in Ref. 1.

Image Processing

Custom Matlab code was written to segment, filter, binarize, and compute sizes of all organelles. Cellular segmentation was semi-automated and varied between datasets. For the confocal images, segmentation was performed by hand with ImageJ. For the camera images, a 2D slice of the cells with a YFP label was filtered and binarized. In each case, the 3D cells were extracted from the field of view to be measured individually.

Two thresholding processes were used, dependent upon the morphology of the organelle. For the globular structures (lipid droplets, peroxisome, and Golgi) the filtering began with a weak Gaussian blur followed by taking the Laplacian of the image. Ultimately, the threshold for binarization was picked by hand and confirmed by eye. For the tubular structures (mitochondria) we used the Hessian based “Frangi Vesselness” filter (available on mathworks.com); the threshold was again picked by hand and confirmed by eye.

After binarization, we used built-in Matlab functions to label the object voxels and segment the individual organelles. Size was computed by counting the voxels in each identified organelle. See Figure 1 for overview of our workflow and quality control metrics.

Mathematical framework for growth with deterministic step sizes

In our mathematical framework (Fig 1a), solve for the dynamics of the proba- bility of a state of organelles in a single cell that undergo the following changes:

I. De novo synthesis of organelles from a given source of constituents within the cell with a constant rate k_{denovo}

$$P(N, \vec{S}_i) \xrightarrow{k_{denovo}} P(N+1, \vec{S'}_{i+1})$$

II. Decay of organelles due to inheritance, maturation, autophagy, etc. at a rate γ per organelle per time:

$$P(N, \vec{S}_i) \xrightarrow{N_\gamma} P(N-1, \vec{S'}_{i-1})$$

III. Creation of two organelles from a single organelle through fission at a rate $k_{fission}$ per organelle per time:

$$P(N, \vec{S}_i) \xrightarrow{N_{k_{fission}}} P(N+1, \vec{S'}_{i+1})$$

IV. Creation of a single organelle through the fusion of two organelles at a rate k_{fusion} per organelle per squared time:

$$P(N, \vec{S}_i) \xrightarrow{N(N-1)k_{fusion}} P(N-1, \vec{S'}_{i-1})$$

V. Organelle size growth at a rate r_{growth} per time:

$$P(N, \vec{S}_i) \xrightarrow{r_{growth}} P(N, \vec{S'}_i)$$

VI. Organelle size decay at a rate k_{decay} per number of organelle constituents (size s) per time:

$$P(N, \vec{S}_i) \xrightarrow{sk_{decay}} P(N, \vec{S'}_i)$$

We initially assume that organelles grow in deterministic increments (packet sizes). In all three limits, we assume that the rates of decay, fission, fusion, and shrinking are Nγ, $Nk_{fission}$, $N(N-1)k_{fusion}$, and S_ik_{shrink} respectively, in which N is the number of organelles and S_i is the size of the ith organelle and S' refers to the size of each organelle in the new probability state. In the case of constant growth, we assume that the growth and de novo synthesis rates are equal to their rate constants respectively (i.e., $r_{denovo} = k_{denovo}$ and $r_{grow} = k_{grow}$). In the negative feedback model, we

assume that the de novo synthesis rate is equal to its rate constants, however the growth rate is constrained by a feedback term

$$r_{growth} = \frac{(target\ size)^h}{1 + (target\ size)^h} k_{growth}$$

in which target size = $\frac{k_{growth}}{k_{decay}}$ and h is the Hill coefficient. Lastly, in the k_{decay} limiting pool model we charactersize the rate for de novo synthesis and organelle growth as $R_{denovo} = k_{denovo}N_{pool}$ and $R_{grow} = k_{grow}N_{pool}$ respectively, in which N_{pool} is the free pool available for the organelles. Additionally, we assume that the pool is replenished by the process of organelle decay and shrinking.

In **Supplementary Fig. 2a-2f** we plot the trajectories of a single cell reaching steady-state for the three limits of our framework, in a regime where the abundance of organelles change through de novo synthesis, fission, and first order decay, and in a regime in which organelle abundance changes solely through fission and fusion.

To obtain additional insight about the three limits of our model, we sweep through a large parameter space and simulate 1000 cells. From each simulation we obtain the slope of the plot of average organelle sizes vs. organelle abun- dance. Finally, we plot the histogram of the recorded slopes by increasing fission rate (purple represents a fission rate of zero and red represents the highest fission rate in our simulations). Comparing the slope histograms, we observe a zero slope for almost all parameter sets in the negative feedback model and a negative slope for all parameter sets used to simulate the limiting pool model. However, we notice that in the constant growth model, the slopes become increasingly negative as fission rates increase (**Supplementary Fig. 2g-2i**). We implement this information to learn about peroxisomal growth. In wildtype yeast, we consider peroxisomes to undergo de novo synthesis, fission, and first order decay. Our measurement of the wildtype data results in a negative correlation between average size and abundance of peroxisomes (**Fig 1n**). However, this can only help us rule out the negative feedback control model, as we expect a negative correlation between number and average organelle size at high fission rates in the constant growth model. In order to determine the correct model to describe peroxisomes, we engineered strains of yeast with their peroxisomal fission factors deleted, while grown in medium rich in long chains of fatty acid. Peroxisomes undergo fission when grown in oleic acid. We observe that even in the strain with the *VPS1* gene deleted (*VPS1* being the quantitatively most significant of all fission factor deletes, Ref. 1), the correlation between the abundance and average peroxisome size is still negative in **Supplementary Fig. 2j-2l**. This argues against constant growth as the underlying mechanism for peroxisomal growth, suggesting that peroxisomes grow from a limited pool of building blocks.

References

1. Mukherji, S. & O'Shea, E. K. Mechanisms of organelle biogenesis govern stochastic fluctuations in organelle abundance. *Elife* 3, e02678 (2014).

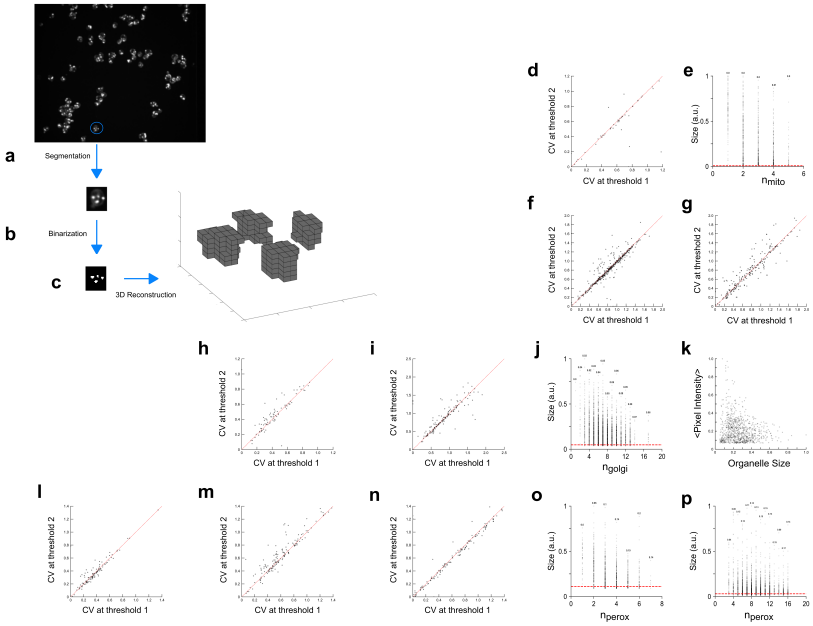

Supplementary Figure 1. After semi-automated segmentation, individual cells are extracted from a given field of view (a). After applying the filters corresponding to the given structure's morphology (globular or tubular), each cell is binarized one z-slice at a time (b). Z-slices are then reconstructed to form a 3D image of the cell and built-in Matlab functions are used to identify individual organelles and count their voxels. In general, our pipeline is robust to choice of threshold, as demonstrated in (d, f-i, l-n) in which we compute the CVs for a population of the given organelle type where Threshold 2 is 10% greater than Threshold 1. For the images collected with a camera, we test the proportion of organelles, cell-blind, fall below the diffraction limit (computed by measuring the size of a diffraction-limited bead). Floating numbers are proportion of each bin that falls below the diffraction limit; in general, this proportion is below 8% though approaches 15-20% for high number bins in peroxisome (e, j, o). Though this does impact our resolution for the smaller sized organelles, if we were capable of resolving smaller organelle sizes then the trends we see would most likely be reinforced.

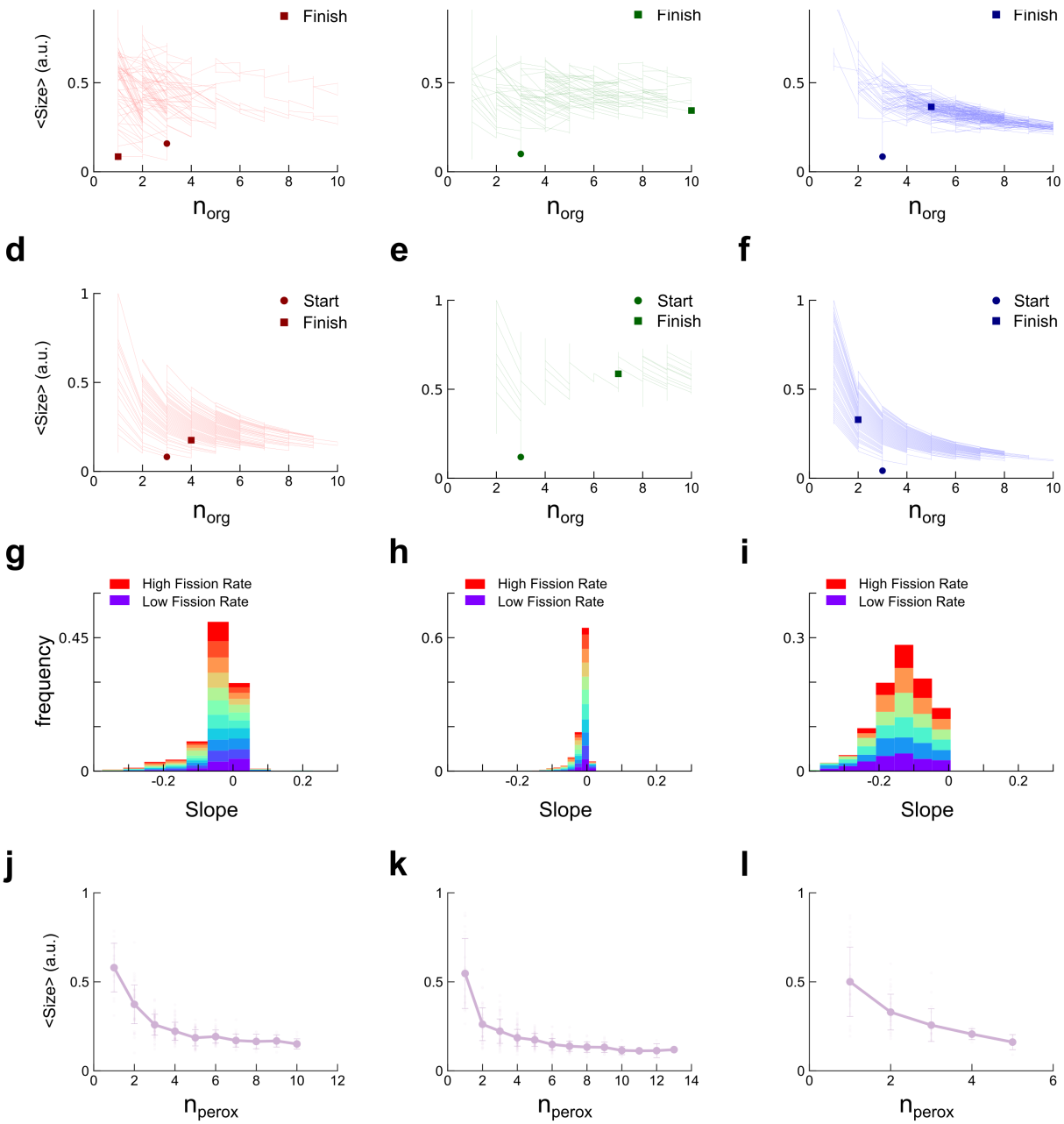

Supplementary Figure 2. In the regime where organelle abundances change through de novo synthesis, fission and first order decay a) trace of a simulated single cell in the limit of constant growth b) negative feedback control, and c) limiting pool, from t=0 (circle) to steady-state (square). In the regime where organelle abundances change through fission and fusion d) trace of a simulated single cell in the limit of constant growth e) negative feedback control, and f) limiting pool, from t=0 (circle) to steady-state (square). Histograms of slopes obtained from sweeping through a large parameter space from $k_{fission} = 0$ to high fission rates for g)the constant growth, h)negative feedback, and i)limiting pool model. Average of mean peroxisome sizes in strains grown in medium rich in oleic acid with their peroxisomal fission factors j) *DNM1*, k)*FIS1*, and l)*VPS1* deleted.

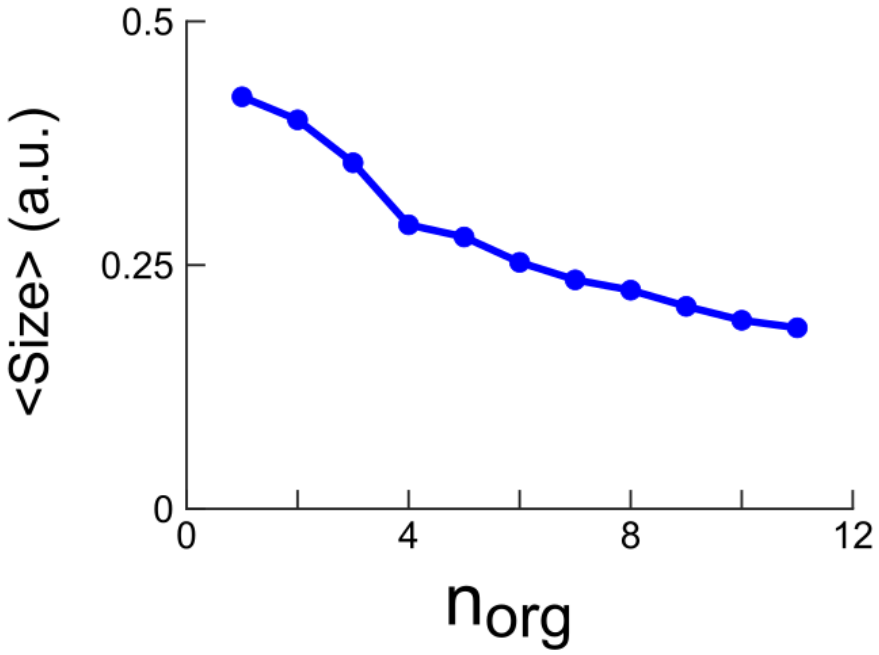

Supplementary Figure 3. We show that our limiting pool model can be extended such that organelle growth occurs in exponentially distributed step sizes at a constant rate kgrowth from a limited pool of building blocks, when number dynamics are significantly slower than growth dynamics, and that this model preserves the negative correlation between organelle abundance and average size.

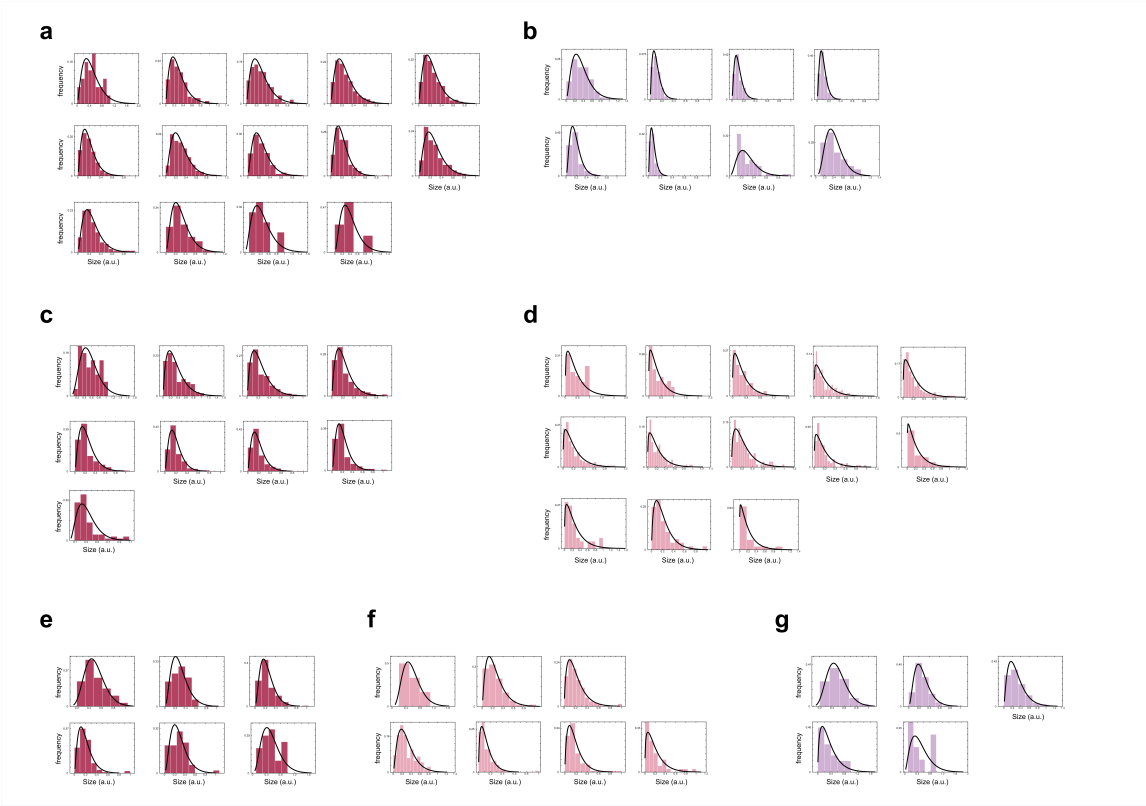

Supplementary Figure 4. distributions and corresponding gamma fits to the a) golgi apparatus in wt strains, b)golgi in strain with *ARF1* deleted, c) lipid droplets grown in glucose, and d) in medium rich in oleic acid, e) peroxisomes in wt yeast strains grown in glucose, f) in medium rich in oleic acid, and g) strain with *VPS1* deleted and grown in medium rich in oleic acid

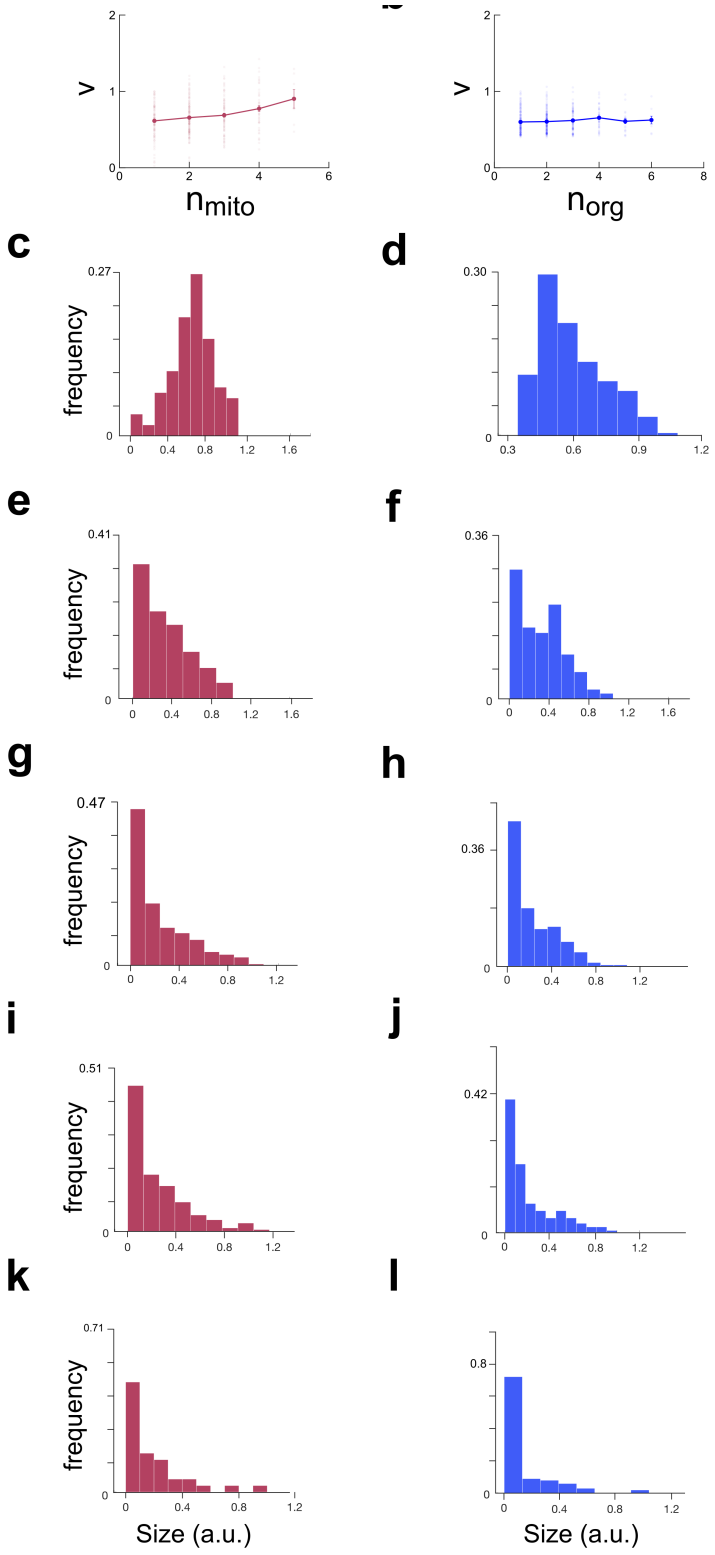

Supplementary Figure 5. V vs. N plot of a) mitochondria (red) and b) result of bursty model(blue) with organelle numbers changing through fission and fusion. c-i) distribution of mitochondria (red) and simulated organelles (blue) sizes in different organelle number bins